1985

Wind–Current Coupling on the Southern Flank of Georges Bank: Variation with Season and Frequency

Marlene Noble

Bradford Butman

See next page for additional authors

Citation/Publisher Attribution

Noble, M., Butman, B., & Wimbush, M. (1985). Wind–Current Coupling on the Southern Flank of Georges Bank: Variation with Season and Frequency. *J. Phys. Oceanogr., 15*, 604-620. doi: 10.1175/1520-0485(1985)015<0604:WCOTSF>2.0.CO;2
Available at: http:/dx.doi.org/10.1175/1520-0485(1985)015<0604:WCOTSF>2.0.CO;2

Wind–Current Coupling on the Southern Flank of Georges Bank: Variation with Season and Frequency

MARLENE NOBLE* AND BRADFORD BUTMAN

U.S. Geological Survey, Woods Hole, MA 02543

MARK WIMBUSH

University of Rhode Island, Narragansett, RI

(Manuscript received 5 April 1984, in final form 8 February 1985)

ABSTRACT

Comparison of several years of current observations on the southern flank of Georges Bank with nearby wind data shows that the wind–current coupling is primarily between longshelf wind stress and longshelf current. The strongest wind–current coupling occurs in winter, when the water column is homogenous. The weakest coupling is in late summer and early fall, when the water column is highly stratified. The coherence and transfer coefficient between longshelf wind and longshelf current is highest for periods between 4 and 12 days, decreasing both for longer periods (out to 56 days) and shorter periods (down to 2 days). Models of the wind–current coupling indicate that a highly damped resonance may exist on Georges Bank and that a smaller current response is expected when the water column is stratified. The observations also indicate that the wind-driven currents on Georges Bank are strongly controlled by friction. The near-surface current moves to the right of wind stress and there is a spring–neap modulation of the wind–current transfer coefficient caused by the modulation of the bottom stress associated with the spring–neap tidal cycle. The longshelf current is linearly related to wind stress and responds almost symmetrically to wind forcing.

1. Introduction

Fluctuating currents on the southern flank of Georges Bank (Fig. 1) can be divided into very energetic tidal currents (with speed around 30 cm s^{-1}; Moody and Butman, 1980) and less energetic subtidal currents. Within the subtidal band (periods longer than 2 days) currents are polarized along isobaths, with most of the current energy in periods between 4 and 12 days. For periods longer than 4 days, subtidal currents and wind stress on the Bank have similar spectral shapes and similar seasonal cycles (Butman and Beardsley, 1985), which suggests that subtidal currents are mainly wind driven.

Many investigators have examined the coherence, and less often the transfer coefficient, between wind stress and subtidal current on Georges Bank and in the Middle Atlantic Bight (600 km to the southwest) (Beardsley and Butman, 1974; Han and Mayer, 1981; Ou *et al.*, 1981; Flagg *et al.*, 1982; Noble *et al.*, 1983). Generally the length of the datasets examined was less than 4 months, and thus the frequency structure of the wind–current coherence could be examined only out to periods of 15 days. These studies have shown that significant wind–current coherence on the shelf exists only between longshelf wind stress and longshelf current. The coherence is low for high frequencies (periods less than 4 days) and increases to an approximately constant amplitude at lower frequencies. The nature of the wind–current coupling for periods longer than about 15 days is not well known.

On the shelf in the Middle Atlantic Bight, the coherence between longshelf wind and current is high for periods from 3 to 15 days (around 0.8). On Georges Bank, wind and current are more weakly coupled (coherence amplitudes around 0.5). However, since the wind field in the Middle Atlantic Bight and over Georges Bank has large spatial scales [O(800) km, Wang, 1979; Noble and Butman, 1979], the wind-driven flow on the Bank is smaller than, but coherent with, wind-driven flow in the Middle Atlantic Bight (Noble *et al.*, 1983). These large spatial scales imply that gross features of the wind-driven flow on Georges Bank may reflect general aspects of the shelf-circulation patterns.

Beginning in 1975, several years of current meter observations were collected at site A, on the southern flank of Georges Bank (Fig. 1). With this long data series, the coupling between wind and current could be examined not only at the very low frequencies (periods out to 56 days), but also as a function of season. No other long-term records of current at one

* Present address: U.S. Geological Survey, Menlo Park, CA 94025.

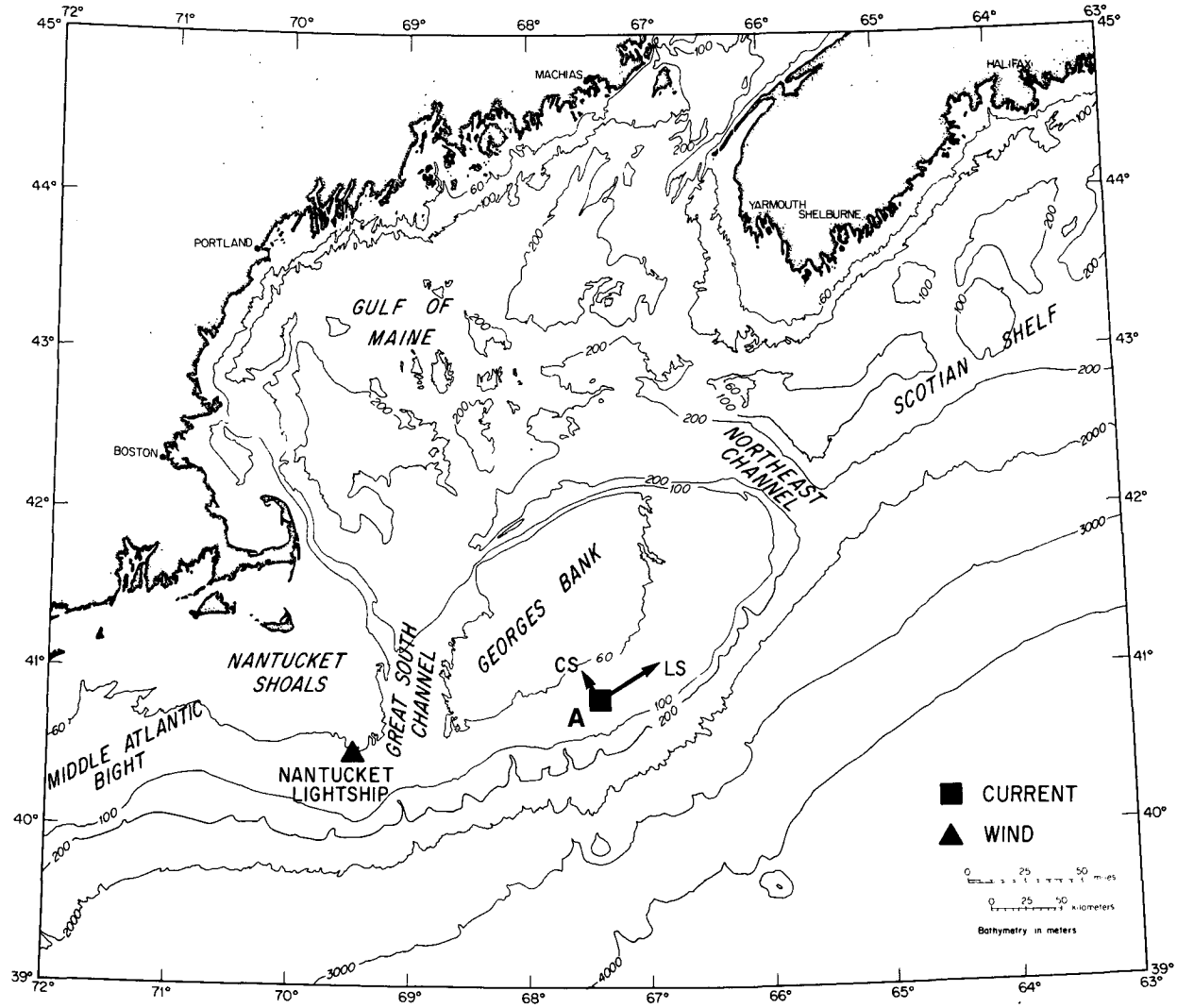

FIG. 1. Location where current and wind data were obtained.

location on the Bank exist. Several shorter-term records of wind and current at various locations around the Bank suggest that the wind-driven current response is strongest in fall (Flagg *et al.*, 1982). Theoretical models also suggest that the strength of the coupling between wind and current changes over the year. The seasonally varying density structure of the water column may introduce a seasonal variation of the wind–current coupling (Brink, 1982; Csanady, 1982). Also, the magnitude of the wind-stress drag coefficient, which is highest when cool air overlies warm water (Roll, 1965), may change during the year. Hence, in late fall or winter, when cold continental air moves over relatively warm shelf water, a stronger coupling between wind stress (when calculated with a time-independent drag coefficient, as is common) and current may occur. To look at the temporal structure of the wind–current coupling on Georges Bank, we have calculated the average wind–current coherence and transfer coefficient every 2 months for the several years of record.

Weak evidence exists for a nonsymmetric response of currents on the New England shelf to northeastward versus southwestward wind stress. On the shelf near 71°W, from data calculated during two major storms which occurred within one month of each other, Beardsley and Butman (1974) suggested that currents associated with a southwestward wind stress were stronger than the currents associated with northeastward wind stress. However, using 6 months of coastal sea level records from stations located in and around the Gulf of Maine, Noble and Butman (1979) inferred that the current response would be strongest for northeastward wind stress. Within this paper, the several years of current and wind stress records are used to examine both the linearity and symmetry of the wind–current coupling as a function of wind-stress direction and amplitude.

2. Dataset

From May 1975 to March 1979, a series of current meter moorings was maintained almost continuously in 85 m of water at site A on the southern flank of Georges Bank (Fig. 1). Current measurements were made at 45 and 75 m below the sea surface for most of the period, and less often at 15 and 84 m (Table 1). For convenience, current observations at depths of 15 m, 45 m, 75 m and 84 m will be referred to as near-surface, middepth, near-bottom and bottom currents, respectively.

Observations of wind speed and direction at Nantucket Lightship were obtained from the National Climatic Center. Nantucket Lightship is an offshore station located about 200 km west of site A (Fig. 1). Since the longshelf scale of wind systems on the New England Continental Shelf is larger than 800 km, the wind at Nantucket Lightship is considered to be representative of the wind on the southern flank of Georges Bank. Wind stress is defined to be:

$$\tau = \tilde{\rho} C_D \mathbf{W}|\mathbf{W}|$$

where $\tilde{\rho}$ is the air density (0.0012 gm cm^{-3}), C_D the wind-stress drag coefficient and $\mathbf{W}$ the wind velocity. The wind-stress drag coefficient increases with wind strength

$$C_D = (0.8 + 0.065|W_{10}|) \times 10^{-3}$$

where $|W_{10}|$ is the wind speed 10 m above the surface in m s^{-1} (Wu, 1980). The wind-stress records use oceanographic conventions; i.e., a north wind blows northward.

All data records were low-pass filtered to remove oscillations that have periods less than 33 hours. Only these subtidal records will be discussed. For convenience, throughout this paper "high frequencies" will refer to fluctuations with periods shorter than 4 days, "midfrequencies" will denote fluctuations with periods between 4 and 12 days, and "low-frequencies" will denote fluctuations with periods longer than 12 days.

The current and wind-stress observations were decomposed into a longshelf/cross-shelf coordinate system. For currents, the longshelf orientation is defined to be the direction of the major axis of the local midwater, subtidal current ellipse (58°), which is within 2° of the large-scale topographic angle. For the wind observations, the longshelf orientation is defined to be parallel to the large-scale Bank topography; the positive longshelf wind-stress direction is chosen to be 60°. In order to determine if 60° is the natural coordinate system for wind stress, the correlation between wind stress and longshelf current was examined as a function of wind-stress angle for the several years of observation at site A. For all data records, the maximum correlation was within 20° of the chosen longshelf wind-stress direction; the minimum correlation was generally below the 95 percent significance level and occurred near the cross-shelf wind-stress direction. Because the difference between the peak correlation amplitude and the correlation amplitude at the defined longshelf wind-stress direction was much less than the error bars around the correlation amplitude (the differences are generally within 0.05), the longshelf/cross-shelf coordinate system for wind stress defined by the gross topography is retained in the subsequent analyses.

TABLE 1. The current meters were deployed in 85 m of water at 40°51.4'N, 67°24.1'W. The instrument name in column one is keyed to the instrument depth and time of observations. The first letter denotes the station location (A), the second digit denotes the sequence of current meters deployed at a similar depth in the same year. When the letter X replaces the sequence number, the current record is a merged record created from several sequential current observations at one depth. The next two digits denote the depth of observation (meters below the sea surface). The numbers following the dash are the last two digits of the launch year.

Instrument	Instrument depth (m)	Observation period	Instrument type[1]
A115-75	15	19 Sep 1975–4 Dec 1975	VACM
A115-77	15	10 Jul 1977–17 Sep 1977	VACM
A115-78	15	13 May 1978–29 Sep 1978	VACM
A145-75	45	10 May 1975–31 Aug 1975	VACM
A245-75	45	19 Sep 1975–14 Jan 1976	VACM
AX45-76	45	18 Aug 1976–6 Jul 1978	VACM
A145-78	45	3 Oct 1978–28 Feb 1979	VACM
A175-75	75	10 May 1975–22 Aug 1975	VACM
A275-75	75	19 Sep 1975–14 Jan 1976	VACM
AX75-76	75	18 Aug 1976–9 Mar 1979	VACM
A184-76	84	6 Dec 1976–17 Mar 1977	TRIPOD
A184-77	84	17 Apr 1977–21 Jun 1977	TRIPOD
A184-78	84	26 Jan 1978–10 May 1978	TRIPOD

[1] VACM Vector averaging current meter.
TRIPOD The tripod has a current meter (small rotor, small vane, vector averaging) and a pressure sensor which rest on a stable bottom platform.

A description of the computation of the statistical quantities which will be used to describe the structure of wind and current is contained in Appendix A. These statistical quantities are wind–current coherence and transfer coefficient (also called frequency response function), autospectra of current and wind stress, the ellipse orientation and stability of currents, and the error bar associated with each statistical parameter. To investigate several aspects of wind–current coupling, the data set has been analyzed either as one long record or has been broken into segments. The full record was used in Sections 3 and 4 to examine the frequency structure, the linearity, and the symmetry of wind–current coupling. In Section 5 the data set was broken into successive 2-month blocks to look at the seasonal cycle in wind and currents. Finally, in Section 6, the records were averaged over times of spring and times of neap tides to estimate the effect of a changing bottom-friction coefficient on the wind-driven currents.

3. Distribution of wind and current statistics by frequency

a. Energy distribution and current ellipse orientation

The energy in longshelf current and longshelf wind stress is large in the midfrequencies and decreases at low frequencies (Fig. 2). At high frequencies, the longshelf current variance is small while the longshelf wind stress remains high. The similarity in the spectral shapes of longshelf current and wind stress in the mid- and low-frequency bands suggests that longshelf wind stress may be an important forcing function for longshelf current. However, the relatively small current variance at high frequencies indicates that the wind–current transfer function is frequency dependent.

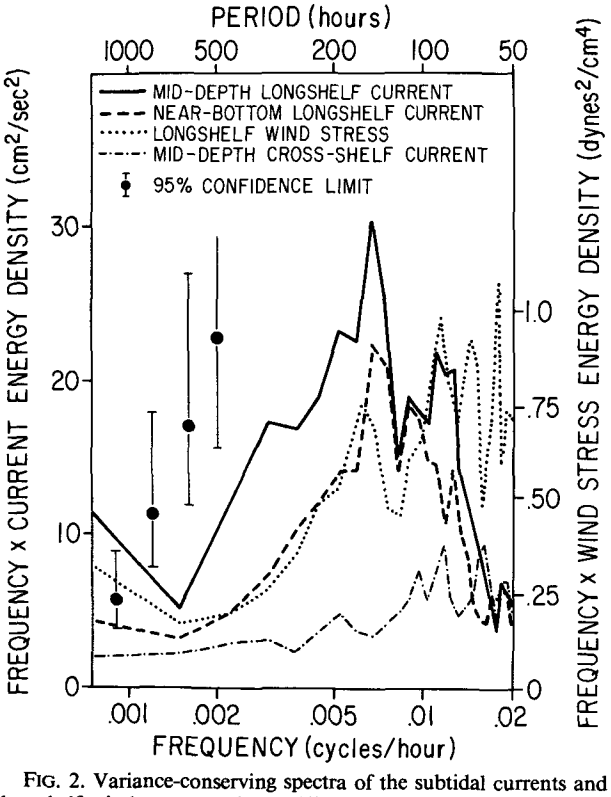

FIG. 2. Variance-conserving spectra of the subtidal currents and longshelf wind stress at site A. The 95-percent confidence limits refer to estimated errors around energy levels represented by the dot.

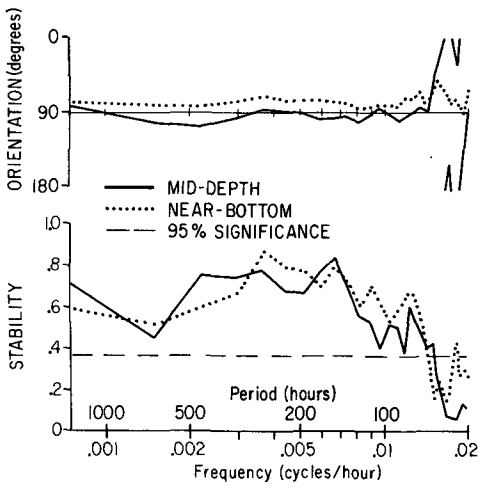

FIG. 3. Ellipse orientation and stability for subtidal current at site A. An orientation of 90° indicates that the major axis of the current ellipse is parallel to the longshelf direction. An orientation less than 90° indicates that the major axis is rotated counterclockwise from the longshelf direction. The significance level is the 95 percent zero-significance level for a coherence with an equal number of degrees of freedom.

The energy in cross-shelf currents is weak in all frequency bands. The cross-shelf wind stress has a variance approximately equal to that of the longshelf wind stress. However, since the cross-shelf wind stress does not drive either long- or cross-shelf currents, it will not be discussed.

Since most of the subtidal current energy is in longshelf currents, it is not surprising that the current ellipse orientation is within 20° of the chosen longshelf direction for middepth and near-bottom currents (Fig. 3). The major axis of the near-bottom current ellipse is generally 20° counterclockwise of the mid-depth axis, consistent with bottom Ekman layer dynamics. The ellipse stability, which has values between 0 and 1 depending on whether the ellipse orientation at a particular frequency varies randomly or is confined to a single direction over the current record, is high for most subtidal frequencies, decreasing only at high frequencies where nearly equal energies are found in the longshelf and cross-shelf currents.

b. Vertical coherence of currents

In the subtidal band, observations of longshelf currents below 45 m are generally representative of currents in the lower half of the water column, for

fluctuations in middepth and near-bottom longshelf current are nearly simultaneous and highly correlated across the entire subtidal frequency range (coherence amplitudes are about 0.8 and phase differences are about −5°, Fig. 4). Even though the midfrequencies contain most of the current variance, the coherence and phase lags for the mid- and low-frequency bands are nearly equal. The small negative phase angles imply that the middepth current slightly leads the near-bottom current, consistent with frictional shelf dynamics.

In contrast, observations of subtidal cross-shelf currents are representative of small vertical scales, for the middepth and near-bottom cross-shelf currents are only weakly coherent (Fig. 4). Minor coherence peaks occur near 1344, 250, 125, and 97 hours, but the periods do not correspond to any cross-shelf spectral peaks.

c. *Wind–current coupling*

The subtidal longshelf wind and longshelf current records are visually correlated. For example, in a representative time span from January to May 1978, the longshelf current events on 10 January, 28 January and 7 February are obviously associated with longshelf wind events (Fig. 5). No obvious peaks corresponding to strong wind events are seen in the cross-shelf current record. However, not all currents are directly wind driven. For example, on 4 April a strong longshelf current pulse is observed when longshelf wind stress is small.

The longshelf wind stress is coherent with longshelf middepth and near-bottom currents over the entire

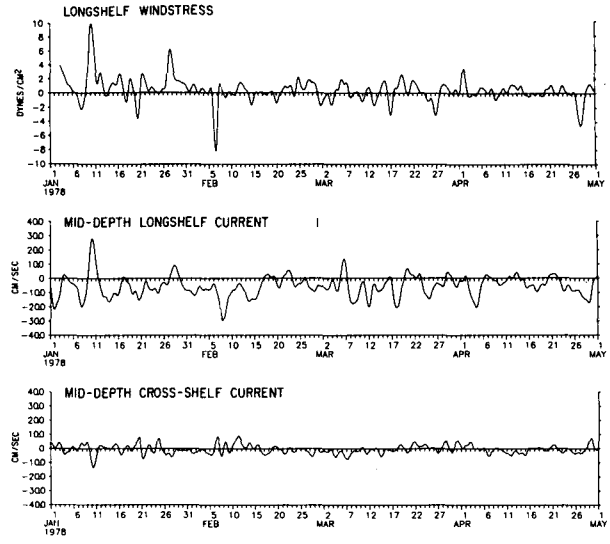

FIG. 5. A representative segment of the subtidal currents and longshelf wind stress at site A. Northeastward movement along the shelf is positive. Northwestward movement onto the shelf is positive.

subtidal band [periods from 2 days (48 hours) to 56 days (1344 hours)], though the coherence does vary with frequency. The largest coherences are found in the midfrequency band (see Fig. 6). An average midfrequency coherence of 0.6 indicates that 35 percent of the midfrequency longshelf current energy is driven by longshelf wind. At low frequencies, the wind stress–current coherent drops to about 0.4 for near-bottom current and is below the 95 percent confidence level for middepth currents. The phase between wind stress and currents changes from negative (currents lead wind) to positive (wind leads currents) within the midfrequency band. Although

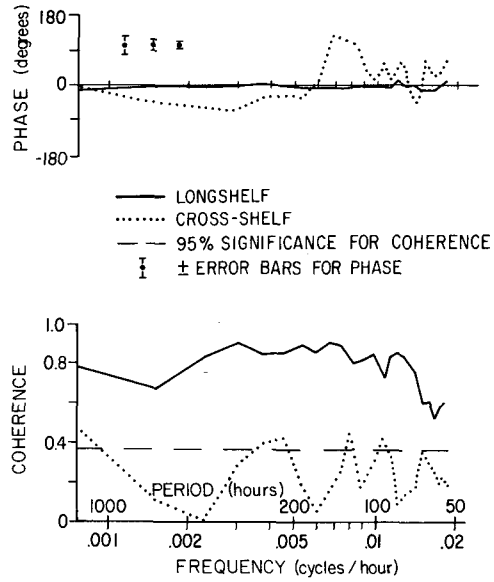

FIG. 4. Phase and coherence between middepth and near-bottom currents. A negative phase implies the middepth current leads the near-bottom current. The phase error bars are for coherence amplitudes of 0.4, 0.6 and 0.8.

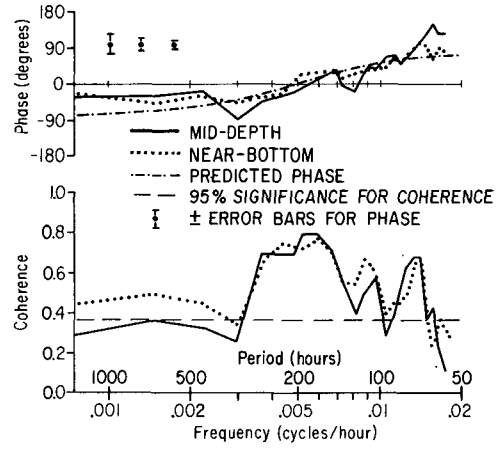

FIG. 6. Phase and coherence between longshelf current and wind stress for the periods from 50 to 1344 h. Wind leads the current when the phase is positive. The predicted phase is the phase angle of a highly damped resonant system responding to a time-varying wind stress (see discussion). The phase error bars are for coherence amplitudes of 0.4, 0.6 and 0.8.

the negative phase angles of the low-frequency near-bottom longshelf currents are not significant at each individual frequency, the average phase for the low-frequency band is $-32 \pm 25°$, indicating that the low-frequency currents do lead the wind stress.

The frequency structure of the wind–current transfer coefficient, which predicts the longshelf current magnitude associated with a one dyn/cm^{-2} longshelf wind stress, is similar to the coherence structure (Figs. 7a, b). The largest transfer coefficients are in the midfrequency band, with amplitudes of 4.5 and 3.5 cm^3/(dyn s) for middepth and near-bottom current, respectively. At low frequencies, the transfer coefficient for near-bottom currents is about half that observed at midfrequencies. At high frequencies, the transfer coefficient is also small.

For the middepth observations, the low-frequency transfer coefficient cannot be reliably estimated because the wind–current coherence is insignificant in the low-frequency band. But the transfer coefficient in the low-frequency band can be shown to be smaller than it is at midfrequencies. One can predict the coherence amplitude from a knowledge of the transfer coefficient amplitude tr, the observed middepth current energy C, and the observed wind-stress energy E (Appendix B). The predicted coherence is

$$\gamma_p^2 = \frac{(tr)^2 E}{C}. \quad (1)$$

If one assumes the magnitude of the middepth transfer coefficient is constant with frequency (i.e., is 4 cm^3/(dyn s), representative of the midfrequency band) then the predicted coherences for the low frequencies γ_p are well above the statistical significance level. The measured coherences are not significant (Table 2). The magnitude of the observed coherence at middepth is consistent with the assumption that the ratio between the transfer coefficients at mid- and low frequencies is about 2, similar to the ratio observed for near-bottom currents.

The frequency structure of the wind–current coupling in the near-surface and bottom layers could not be examined, for the current records are too short. However, when the statistical parameters are averaged across the subtidal band, the near-surface currents are occasionally coherent with longshelf wind stress, and move to the right of the wind (Table 3). The transfer coefficient between near-surface cross-shelf current and longshelf wind stress is about 3.5 cm^3/(dyn s). For the two time periods when no wind–current coherence is observed in the near-surface layer, the near-surface current variance is large but the wind stress is weak. Hence, a wind-driven current of 3.5 cm^3/(dyn s) would be an insignificant portion of the total near-surface current field, and the observed coherences would be below significance levels. The wind-driven bottom currents move nearly parallel to the longshelf wind stress. A slight veering to the left is observed, but the veering angle may not be statistically significant, as the range of veering angles in two out of three observations spans the longshelf direction (60°T).

TABLE 2. Observed and predicted coherence between longshelf wind stress and longshelf current at 45 m.

Period (h)	Observed coherence	Predicted* coherence	Significance level
1344	0.32	0.76	0.39
672	0.39	0.60	0.39
448	0.36	0.69	0.39
336	0.26	0.77	0.39

* Transfer coefficient assumed to be 4 cm^3/(dyn s).

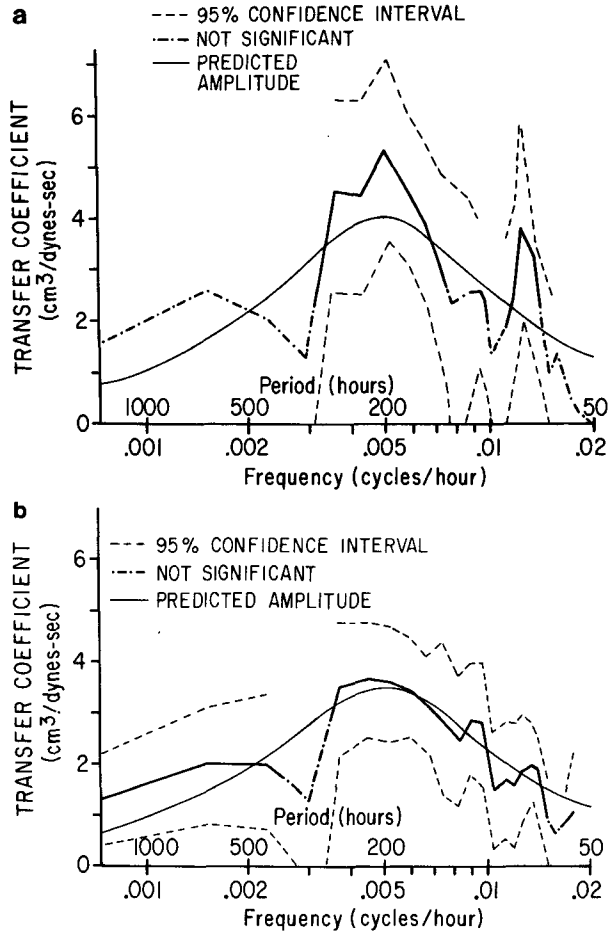

FIG. 7. Transfer coefficient between longshelf wind stress and middepth (a) and near-bottom (b) longshelf current. The phase of the transfer coefficient is the same as the phase for the coherence and is depicted in Fig. 6. The predicted amplitude is the response of a highly damped resonant system to a time-varying unit-amplitude wind stress (see discussion). The steady-state response is 4.4 cm^3/(dyn s) for middepth and 3.8 cm^3/(dyn s) for near-bottom current.

TABLE 3. Coherence, transfer coefficients and veering angles for near-surface and bottom currrents with longshelf wind stress. Positive phase implies winds lead currents. Since the topographic angle for longshelf wind stress is 60°, veering angles larger than 60° imply the currents move to the right of wind stress. A description of the veering angle computation is given in Appendix B.

Instrument	Time (YrMoDy–YrMoDy)	Depth (m)	Current veering Angle	Current veering Range (deg)	Coherence	Phase (h)	Transfer coefficient [cm^3/(dyn s)]
A115-75	750919–751123	15	135	115–150	0.62	18	4.0 ± 2.0
A115-77	770710–770914	15	—	—	—	—	—
A115-78	780513–780717	15	130	115–145	0.52	9	2.8 ± 1.7
A115-78	780701–780904	15	—	—	—	—	—
A184-76	761206–770315	84	55	35–75	0.42	3	1.3 ± 1.1
A184-77	770417–770611	84	40	30–50	0.63	0	2.1 ± 1.0
A184-78	780126–780504	84	55	45–90	0.42	0	1.5 ± 1.2

4. The linearity and symmetry of the current response to wind stress

To determine the linearity of the current response to wind stress, the longshelf currents were sorted into bins determined by longshelf wind-stress direction and amplitude (Fig. 8). For positive wind stress, the averaged longshelf current amplitude is a tight linear function of wind-stress amplitude. For negative wind stress, there is appreciable scatter about a linear regression line. However, the additional scatter does not indicate that the longshelf current response to negative wind is necessarily more variable, because for this data set there were twice as many positive wind-stress events as negative. Thus, the averaged current response to negative wind stress is expected to be statistically noisier.

To determine the symmetry of the response of longshelf current to longshelf wind stress, the regression between currents and positive (northeastward) and negative (southwestward) wind stress was calculated (Table 4). A regression was also calculated for the wind stress and the average current amplitude in each of the bins depicted in Fig. 8. Both regressions have nearly the same values for the slope and intercept of the current response to wind stress [within 0.2 cm^3/(dyn s)] and both suggest that there may be a slightly stronger current response to northeastward wind stress. However, the data are not conclusive at the 95 percent significance level. The error bars on the slopes of the current response to northeastward versus southwestward winds overlap (2.1 ± 0.5 versus 1.4 ± 0.9 for middepth current) and a straight line, with a slope equal to that observed for positive sorted current, will lie within the error bars around the negative sorted current. Since the sorted current has been averaged over bins in wind space, much of the noise has been removed. Hence, the correlation coefficients in Table 4 between longshelf wind stress and current are higher for the sorted current than for the basic current.

The longshelf wind-stress/longshelf current sorts indicate that currents are linearly related to wind stress and that the response to positive and negative wind stress is nearly symmetric, at least to the statistical accuracy of the dataset. Hence, the assumptions of linearity and symmetry intrinsic to the coherence analysis described in this paper are reasonably satisfied.

It is interesting to note that the transport of water and suspended material alongshelf during storms may be a function of wind-stress direction, even though the wind-generated currents are not. The mean longshelf current on Georges Bank flows southwestward along the shelf, with an amplitude of 9 cm s^{-1} middepth and 4 cm s^{-1} near the bottom. Currents generated by southwestward winds enhance the mean

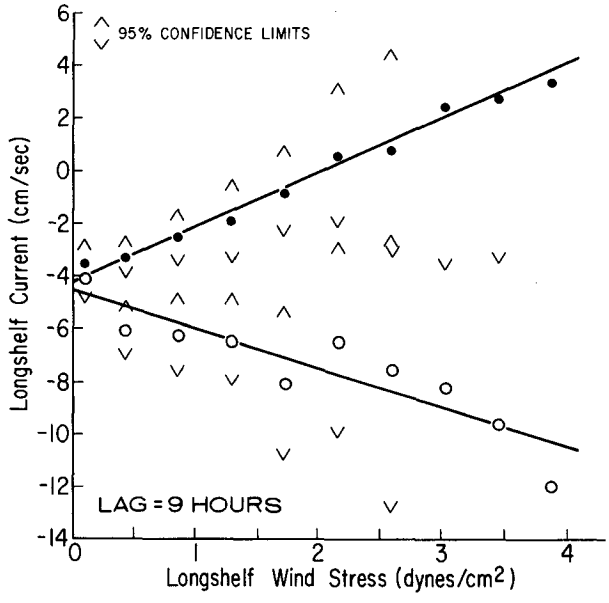

FIG. 8. Subtidal longshelf currents sorted by longshelf wind-stress direction and amplitude. The dark circles represent bins of northeastward wind stress; open circles are for southwestward wind stress. The error bars around the sorted currents are not depicted when they are offscale. The sorted currents lag the wind by 9 h. The slope and intercept of the regression lines are given in Table 4. The sorts for middepth and near-bottom current are very similar and only near-bottom currents are depicted.

TABLE 4. Regression of longshelf current on longshelf wind stress. Northeastward winds are positive. Southwestward winds are negative. The currents lag the wind by 9 h. The sorted current was averaged into bins of wind direction and speed. The basic current was not.

		Basic current			Sorted current		
Wind direction	Current	Slope [cm^3/(dyn s)]	Intercept (cm s^{-1})	Correlation	Slope [cm^3/(dyn s)]	Intercept (cm s^{-1})	Correlation
Positive	Middepth	2.1 ± 0.5	−9	0.37	2.1	−9	0.96
Negative	Middepth	1.4 ± 0.9	−10	0.20	1.2	−10	0.74
Positive	Near-bottom	1.8 ± 0.4	−4	0.41	1.9	−4	0.99
Negative	Near-bottom	1.5 ± 0.6	−5	0.30	1.5	−5	0.90

current, transporting water and suspended material southwestward along the shelf. Northeastward currents oppose the mean. If the mean current were constant over the year, only strong northeastward wind-stress events, with amplitudes exceeding 4 dyn cm^{-2} for middepth currents, 2 dyn cm^{-2} for near-bottom current, would generate a northeastward current. However, the asymmetry in net transport is expected to have a seasonal cycle, for the monthly mean current at middepth changes with season (Butman and Beardsley, 1985). The monthly mean southwestward flow is strongest in summer (−11 to −12 cm s^{-1}) and weakest in winter (−5 to −6 cm s^{-1}). Since winter storms often exceed 2 to 3 dyn cm^{-2} (the amplitude needed to reverse a −5 to −6 cm s^{-1} current), northeastward current pulses are often associated with northeastward wind events.

5. Seasonal variation of wind stress and currents

At site A, the density structure of the water column varies with season (Fig. 9). From December to April, the water column is weakly stratified. From May to mid-September, a strong thermocline develops between 20 and 40 m; thus strong density gradients exist between the sea surface and the depth of the near-surface observation and between the depths of the near-surface and middepth observations. Between the depths of the middepth and near-bottom observations, the water column is weakly stratified. From September to mid-December the cooling surface waters sink, overturning the water column. Because density patterns change with season, the subtidal current field may also vary with season.

To examine seasonal current variability, the subtidal current parameters (variance, orientation, vertical coherence, and wind–current statistics), were computed in 2-month blocks. For statistical stability, all current parameters have been averaged over the periods between 2.4 and 22 days (see Appendix A).

a. Seasonal patterns for wind and current variance

The variances in the longshelf current and wind stress are strong functions of season and have very similar time histories (Fig. 10). The most energetic period is from late fall through winter. The least energetic period is in summer. The correlation between the variances of longshelf wind stress and currents is high, about 0.70 and 0.75 for middepth and near-bottom currents, respectively. Wind-stress variance often increases simultaneously with current variance. However, in the early fall of 1977, the middepth longshelf current variance increased dramatically when no associated increase in wind-stress variance was observed. At that time, Gulf Stream

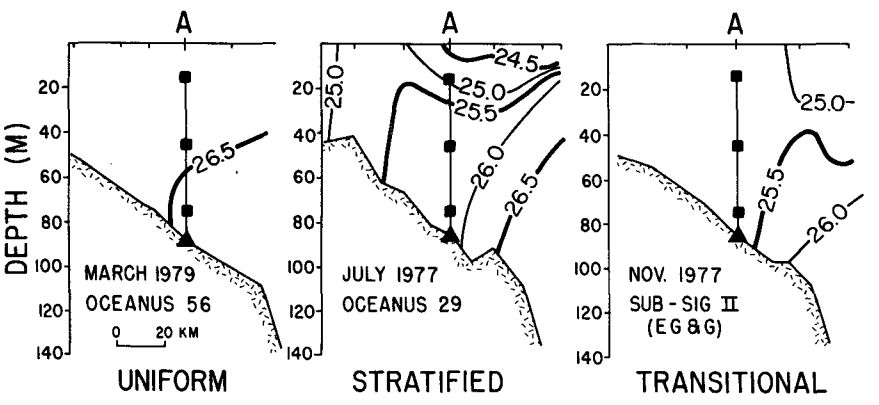

FIG. 9. Schematic hydrographic sections across the southern flank of Georges Bank. The yearly cycle in the density field can be roughly divided into 3 seasons: a uniform season from December through April; a stratified season from May through mid-September; and a transitional season from mid-September to December.

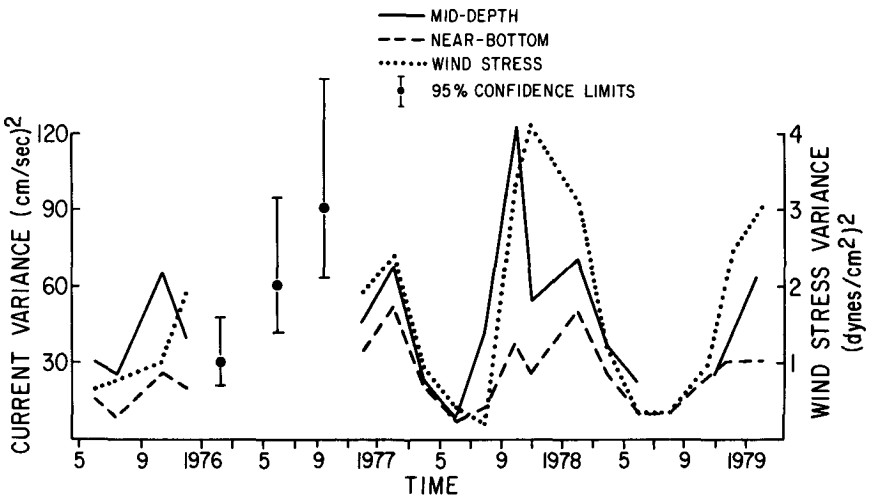

FIG. 10. The temporal change of the variance in the subtidal longshelf currents and wind stress. The variance was computed for 2-month sequential data blocks, as described in Appendix A.

Meander "R" and Eddy "Q" were offshelf near the mooring site and may have enhanced the shelf current variance.

The orientations of the current ellipses are within 25° of the longshelf orientation throughout the several years of observations (Fig. 11). The near-bottom current is generally 10–20° counterclockwise of the middepth current. There is no obvious seasonal pattern in the preferred ellipse orientation. However, the stability of the orientation does vary with season. During the late fall and winter, when current variance is high, the ellipse orientations are very stable. The ellipse stability decreases in summer–early fall, when current variances are low and stratification is high.

b. Seasonal patterns for vertical current coherence

The vertical coherences between the longshelf subtidal currents also vary with season (Fig. 12a). The

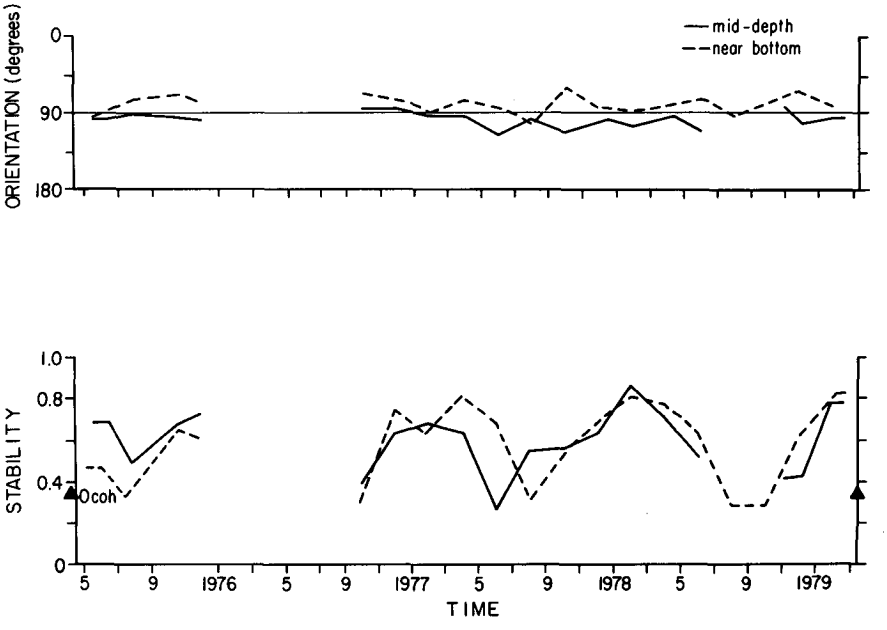

FIG. 11. The temporal change of the ellipse orientation and stability of the subtidal currents at site A. An orientation of 90° indicates that the major axis of the current ellipse is parallel to the longshelf direction. An orientation less than 90° indicates that the ellipse axis is rotated counterclockwise from the longshelf direction. The ellipse parameters were computed for 2-month sequential data blocks as described in Appendix A. The solid triangle is the 95 percent zero-significance level for a coherence with an equal number of degrees of freedom.

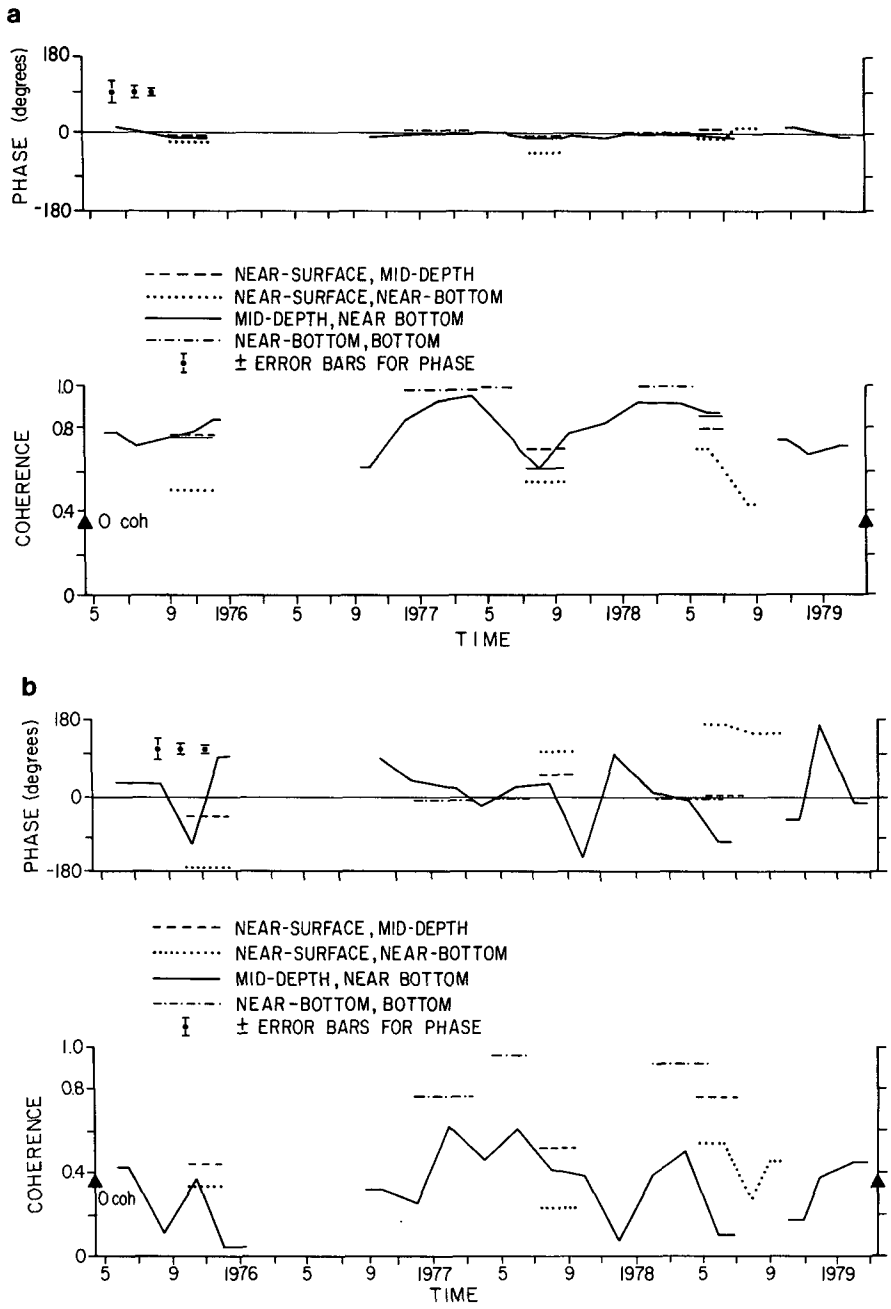

FIG. 12. The temporal change of the coherences among subtidal longshelf currents (a) and cross-shelf currents (b). A negative phase indicates that the upper instrument leads the lower. The phase error bars are for coherence amplitudes of 0.4, 0.6, and 0.8. The coherences were computed for 2-month sequential data blocks as described in Appendix A. The solid triangle is the 95-percent significance level for 0 coherence.

coherence between middepth and near-bottom currents is high in the late fall and throughout the winter (approximately 0.9). Lower coherences are observed in the summer and early fall. The currents within 10 meters of the bottom are very coherent during the several months observations that exist (coherence amplitudes of 0.98). Unfortunately the only near-surface records were obtained during the late summer and early fall, so information on the seasonal structure of currents over the total water column is limited. The available observations suggest that coherences between near-surface and middepth, and between middepth and near-bottom currents are about the same amplitude. The lowest coherences are always

between the near-surface and near-bottom instruments, which have the largest vertical separations.

The coherence between the middepth and near-bottom cross-shelf currents is moderate (Fig. 12b). During the winter months the coherence is around 0.5, in summer it approaches zero significance, and in the fall it is not significant. Only cross-shelf currents within 10 m of the seabed are highly coherent (coherences between 0.77 and 0.98). The coherence between near-surface and middepth cross-shelf currents varies in time. However, the distribution of the observations throughout the year is too limited to determine the seasonal pattern. The phase between near-surface and middepth observations is approximately zero, indicating that the near-surface and middepth currents fluctuate together. The near-surface and near-bottom cross-shelf currents are generally incoherent during the summer and fall. In the summer of 1978, the phase angle during a short period of coherence over the mooring indicates that the surface and bottom cross-shelf currents are moving in opposite directions.

c. *Seasonal patterns for wind–current coupling*

Similar seasonal patterns exist for the coherence and transfer coefficients between longshelf wind stress and longshelf middepth or near-bottom currents (Figs. 13a, b). From winter through early summer, the coherence and transfer-coefficient amplitudes are fairly uniform. The coherence is not significant in midsummer, but since summer wind stress is small this does not necessarily imply that the wind–current coupling in midsummer is weaker than in winter. In fact, the predicted summer coherence, based on the average winter transfer coefficient and on the summer wind-stress variance [Eq. (1), Appendix B], is below the zero-significance level, consistent with observations. However, in late summer and throughout the fall, the wind-stress increases, and the predicted coherences are well above the zero-significance level. Since the measured coherences are not significant, it is inferred that the wind–current coupling in fall is smaller than in winter. The Gulf Stream Meander "R" and Eddy "Q" were south of the mooring site in September 1977 and may have altered the wind–current coherence statistics. However, the presence of eddies cannot fully explain the lack of wind–current coherence in fall, because the wind and current remained incoherent after the eddies have left the mooring site. Wind–current coherence minima are also observed during the fall of other years for which we have data (1975, 1978).

6. Spring–neap variations of the wind–current transfer coefficient

Often bottom friction is parameterized by a quadratic drag law, where bottom stress is proportional to current velocity and current speed. In the presence of strong tides, the nonlinearity of the drag law implies that an interaction exists between tidal currents and the subtidal flow. Since subtidal currents on Georges Bank are much smaller than tidal currents, the quadratic stress law can be linearized to:

$$\tau_b = \rho c_d |U_t| U_s$$

where ρ is water density, c_d the bottom drag coefficient, U_t the tidal amplitude, and U_s the subtidal current. The tidal current amplitude is modulated on a 354 h (fortnightly) and a 661 h (monthly) cycle, as the tidal component pairs M_2, S_2 and M_2, N_2 beat against each other. Spring tides are the maximum amplitude of either the 354 or 661 h period, and neap tides are the minimum amplitude.

The bottom resistance coefficient ($\rho c_d |U_t|$) has a spring–neap cycle, since it is a function of tidal amplitude. Hence the wind-driven current amplitude may also have a spring–neap cycle, as the current adjusts to changes in the amplitude of the resistance coefficient. For a constant ratio between wind stress and bottom stress, the wind-driven current (and transfer coefficient) will be large when the resistance coefficient is small (neap tides) and small when the resistance coefficient is large (spring tides).

The wind–current transfer coefficients were computed at spring and neap tides. The time of spring and neap currents was determined from the phases of the M_2, N_2 and S_2 tidal currents at site A (Moody *et al.*, 1984). Hanning windows 354 and 661 h long were applied to the subtidal wind–current datasets, with the peak amplitude of the window centered at the time of spring or of neap currents.

During neap tidal periods, the transfer coefficients are 20–40 percent larger than during spring tides (Table 5). The error bars for the spring/neap transfer coefficients do overlap; even several years of data are not sufficient to separate statistically the current response. However the observed ratios between the transfer coefficient amplitudes at spring and neap periods are in good agreement with the predicted ratios (which are based on the observed spring/neap tidal current or pressure amplitudes, when the intrinsic averaging of a Hanning window is accounted for).

7. Discussion

The coupling between wind and current on Georges Bank is not well understood, mainly because of the complex topography in the region. The large, shallow submarine bank (with depths less than 30 m) forms the seaward edge of the Gulf of Maine and is separated from the Scotian Shelf by the deep Northeast Channel (Fig. 1). Several models of wind-forced current in this region have simplified the Bank topography. The Bank is represented as a continental shelf (Noble *et al.*, 1983), as an infinitely long submarine bank

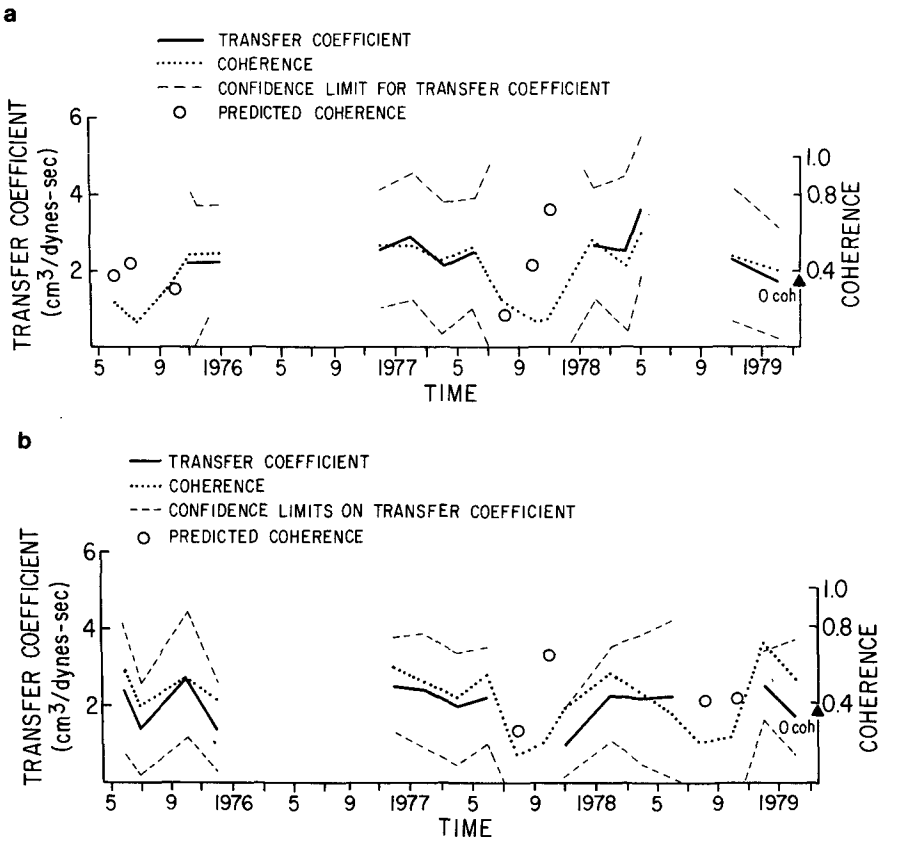

FIG. 13. The temporal change of the coherence and transfer coefficients between longshelf wind stress and middepth longshelf current (a) and near-bottom current (b). The parameters were computed for 2-month sequential data blocks as described in Appendix A. The predicted coherence assumes the amplitude of the transfer coefficient for a particular 2-month segment was 2.6 $cm^3/(dyn\ s)$ for middepth current and 2.2 $cm^3/(dyn\ s)$ for near-bottom current. The solid triangle is the 95-percent significance level for 0 coherence.

(Brink, 1983) or as a part of the Gulf of Maine (Csanady, 1974). Each of these models predicts that longshelf wind stress will drive a longshelf current, consistent with observations (for a more detailed discussion of predicted versus observed current amplitude, see Noble *et al.*, 1983). A three-dimensional, numerical model of wind-driven currents, which incorporates both the complex topography of the Georges Bank/Gulf of Maine region and the strong tides that exist over the Bank, also predicts that currents respond mainly to the longshelf component of wind stress (Isaji *et al.*, 1981). On the southern flank of the Bank, in 117 m of water, the numerical model predicts a one-dyne wind stress will drive a 3

TABLE 5. The transfer coefficients during times of spring or times of neap tides have been averaged over the periods from 60 to 350 h. The amplitudes of the tidal constituents at site A are: M_2 = 32 cm s^{-1} (39 cm), N_2 = 6.5 cm s^{-1} (9.6 cm), S_2 = 4.7 cm s^{-1} (8.7 cm). The first values are for current amplitudes. The numbers in parentheses are for pressure amplitudes. Since current observations are generally noisier than tidal pressure observations, the amplitude ratios for pressure may be more representative of the actual current ratios than the measured current ratios. The lower value for the predicted current ratio (1.2) is computed from observation of tidal current amplitude. The higher number (1.3) is from pressure observations.

Period (h)	Depth (m)	Transfer coefficient [$cm^3/(dyn\ s)$]		Coherence squared		Spring/neap ratio	
		Spring	Neap	Spring	Neap	Observed	Predicted
354	45	1.4 ± 0.5	1.9 ± 0.5	0.07	0.12	1.3	1.2–1.3
354	75	1.5 ± 0.3	1.8 ± 0.3	0.15	0.20	1.2	1.2–1.3
661	45	1.5 ± 0.5	2.2 ± 0.6	0.10	0.15	1.4	1.2–1.3
661	75	1.7 ± 0.4	2.2 ± 0.4	0.18	0.26	1.3	1.2–1.3

cm s^{-1} depth-averaged current, in rough agreement with the observed, middepth transfer coefficient at site A. The observed interaction between tidal and wind-driven flow is evident in the numerical model, for wind-driven currents approximately double in amplitude when tides are not included. The predicted wind-driven transport is largest over the slope (depths greater than 200 m). It is not known if strong wind-driven flow exists over the slope, but preliminary data suggest that wind-driven slope currents are weaker than shelf currents (Butman *et al.*, 1983).

The above models are for an imposed, steady wind and do not address the frequency structure of the wind–current coupling. The predicted wind–current transfer coefficients are constant for periods longer than the transient spinup time of the system (usually less than 2 days on the 80–100-m isobath). However, the observed coupling is strong in the midfrequency band and is weaker for both high and low frequencies. Phases are negative for frequencies less than about 0.005 cycles/hour and positive for higher frequencies. This frequency structure suggests that a resonance may exist in the wind–current coupling on Georges Bank.

The equation used to model a resonant feature in the Georges Bank/Gulf of Maine system should be three-dimensional and include the complex topography and boundary conditions appropriate to the region. However, a simple local model of wind-driven current, which assumes a resonance exists, can be used to characterize a resonant feature at one location. Let a simplification of the vertically integrated longshelf wind-driven momentum equation be a basis for the model equation.

$$h\frac{\partial v}{\partial t} + rV + b\int V dt = T/\rho. \qquad (2)$$

Here V is the longshelf current, T the wind stress, h the depth and r is the bottom resistance coefficient (hence rV is bottom stress). The third term in the equation is the hypothesized restoring force for the resonance and is proportional to the water displaced by wind stress.

Equation (2) represents a damped harmonic oscillator for the integral of velocity (or displacement). For a wind stress of

$$T = T_0 e^{-i\omega t},$$

the current response is

$$V = \frac{\omega T_0 e^{-i(\omega t-\theta)}}{[h(\omega^2 - \omega_0{}^2)^2 + 4\gamma^2\omega^2]^{1/2}}$$

where

$$\gamma = r/2h, \quad \omega_0 = (b/h)^{1/2}$$

and the phase

$$\theta = \tan^{-1}[2\gamma\omega/(\omega_0{}^2 - \omega^2)] - \pi/2.$$

Note, with this phase convention, the phase crosses zero at $\omega = \omega_0$. The natural frequency and hence the unknown coefficient b, can be determined from the data set.

At site A, the depth is 85 m, the resistance coefficient is 0.1 cm s^{-1} (Noble *et al.*, 1983) and $\omega_0 = 2\pi * 0.005$ rph (Fig. 6). The ratio of the decay time to the free-oscillation frequency

$$\frac{\gamma}{(\omega_0{}^2 - \gamma^2)^{1/2}}$$

is 0.9. At this location, free oscillations would decay within one cycle.

For illustrative purposes, the amplitude and phase of the predicted current are depicted (Figs. 6 and 7a, b). The predicted current amplitudes in Fig. 7 are 40 percent of the amplitudes given by the harmonic model.

Although the data suggest that a resonance occurs in the wind-driven coupling, two other phenomena which could introduce a frequency dependence in the wind–current transfer coefficient need to be considered.

1) Because the wind-driven currents on the Bank are part of a shelfwide response to a large-scale wind system, a smaller wind–current coupling may occur at frequencies where the wind systems are not spatially coherent. The spatial structure of the wind field was examined as a function of frequency between New Jersey and Nantucket Lightship (Fig. 14). There is no decrease in the spatial coherence of wind stress at low or at high frequencies. Hence the smaller wind–current transfer coefficient in these frequency bands

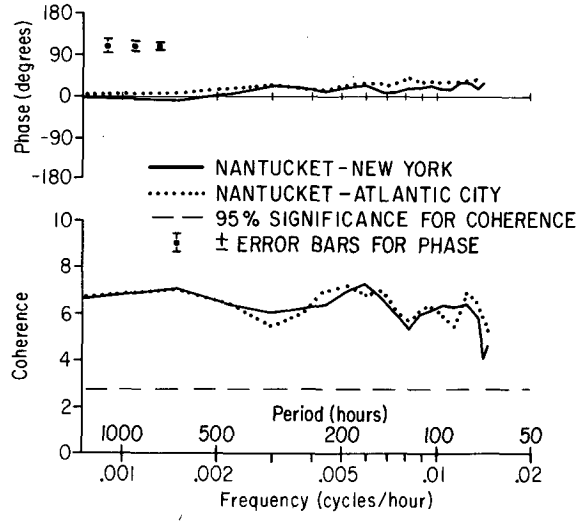

FIG. 14. The phase and coherence among wind-stress records from Atlantic City, New Jersey, JFK International Airport, New York, and Nantucket Lightship. Atlantic City and Nantucket Lightship are separated by 450 km. A positive phase indicates that the second station in a station pair leads the first.

cannot be attributed to a spatially incoherent wind field.

2) The variance of temperature at site A increases markedly for periods longer than 8 days (192 hours) (Fig. 15), indicating that the density field may be nonstationary at these low frequencies. Since the wind–current coupling is expected to be a function of stratification, the averaging of the coupling over a changing environment, which occurs at low frequencies, could also be responsible for the observed low-frequency degradation of the wind–current transfer coefficient.

On the Bank, the seasonal variation and frequency structure of the longshelf current and longshelf wind-stress variances are similar over the several years of observations. The energy in the wind and current is highest in the late fall and winter months, lowest in summer, and largest in the midfrequency bands. The tracking of wind and current variance is somewhat surprising, since only 20–30 percent of the current energy is linearly forced by local wind stress. If the remaining current energy were constant in time, or varied in a seasonal cycle unrelated to that of wind stress, the ratio between current energy in winter (when winds are strong) to current energy in summer (when winds are weak) would be less than is observed. Evidently, a significant nonlinear, nonlocal, or nonstationary coupling occurs between winds and currents on the southern flank of the Bank. Freely propagating events, which are set up by wind events, but are not locally forced by wind, could account for part of the indirect wind–current coupling. Freely propagating events, incoherent with wind stress, were observed to occur after winter storms on Georges Bank (Noble *et al.*, 1983) and have been observed to propagate southwestward on the New York Shelf (Ou *et al.*, 1981). The energy in the freely propagating events on the Bank varied with time but, on average, was approximately equal to the energy in directly wind-forced current. During the winter of 1978, wind-forced currents and freely propagating events together accounted for 75 percent of the longshelf current energy on Georges Bank.

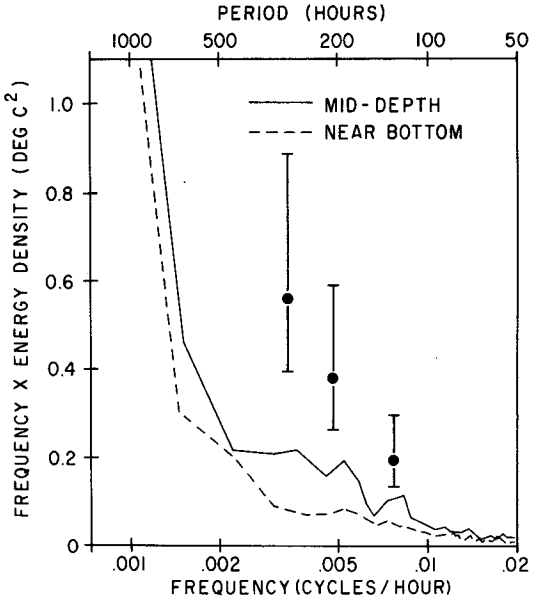

FIG. 15. Variance-conserving spectra of the middepth and near-bottom temperature at site A. The range bars represent 95-percent confidence limits for a variance centered on a solid circle.

The wind–current coherence and transfer coefficients vary with season, indicating that a seasonal variation occurs in the linear coupling between wind and current. Since density in the shelf waters also changes on a seasonal cycle, stratification of the water column may be partly responsible for the seasonal cycle in wind–current coupling. Brink's (1982) model of wind-forced currents on the frictional continental shelf and slope of Peru indicates that, in the presence of strong stratification, 1) the shelf currents are relatively barotropic in that only small changes occur in the amplitude and phase of the current water depths and 2) the coupling between wind and currents is reduced by about 30 percent. The observed wind-forced currents on Georges Bank show some of the general characteristics predicted for shelf currents off Peru. The wind-forced middepth and near-bottom currents are approximately barotropic, in that their respective transfer coefficients have nearly the same amplitude and approximately the same phase throughout the year. However, it cannot be clearly established whether the seasonal change in the transfer coefficient on Georges Bank is due to changes in stratification, since no change in the transfer coefficient amplitude is observed from winter through early summer, when surface waters become stratified. During times of highest stratification, summer winds are weak and the transfer coefficient could not be estimated. However, water on the Bank is stratified well into the fall, when a definite decrease in transfer coefficient is observed. If the amplitude of the fall transfer coefficient were 70 percent of the observed winter value, then the wind–current coherences that can be calculated from the observed amplitudes of wind stress and current in the fall [Eq. (1)] would be below the zero-significance level, consistent with the observed lack of wind–current coherence in the fall.

8. Summary

The subtidal currents on the southern flank of Georges Bank are polarized along isobaths; the longshelf currents contain most of the current energy. In winter, when the water column is unstratified, the longshelf currents are barotropic. The coherence between middepth and near-bottom currents in winter is greater than 0.90 and winter phase angles are less

than 10°. In summer, when the water column is highly stratified, the vertical coherence of the longshelf currents is near 0.6, with slightly larger phase angles than are usually found in winter. The seasonal cycles of the longshelf current and wind-stress variances are approximately in phase. High current and wind-stress energies occur in late fall and winter; summer energies are low. The midfrequency band contains most of the longshelf current energy, but the wind energy is spread over both the mid- and high-frequency bands.

The coupling between wind and current is a function of both frequency and season. The largest coherences (0.75) and transfer coefficients [4.5 cm^3/(dyn s) and 3.5 cm^3/(dyn) for middepth and near-bottom currents, respectively] are found in the midfrequency band. The coupling is much weaker at low and at high frequencies. The phases at low frequencies are negative and are positive at high frequencies. The decrease in transfer coefficient amplitudes and the change in phase angles can be described qualitatively by a simple model of a highly-damped resonant system, responding to a time-varying force. The band-averaged coherence and transfer coefficients are largest in winter and smallest in late summer–early fall. The seasonal decrease in the wind–current coupling may be associated with the seasonal increase in the stratification.

Frictional effects are evident in the wind–current coupling on Georges Bank. Near-surface currents move to the right of the longshelf wind and near-bottom currents are rotated 20° counterclockwise from middepth currents. These trends are consistent with Ekman layer dynamics. The spring–neap modulation of the bottom-drag coefficient for subtidal currents, caused by the modulation of the semidiurnal tidal amplitude, induces a spring–neap modulation in the wind–current coupling. The wind–current transfer coefficient is largest for neap tides and smallest for spring tides.

Longshelf current appears to respond linearly to longshelf wind stress. The slope of the current response to northeastward winds is slightly larger than the slope for southwestward winds, but the difference in slopes is not significant at the 95 percent level. However, it is interesting to note that the slight asymmetry is of the same sign as was previously found with coastal sea-level records in the Georges Bank–Gulf of Maine region.

Acknowledgments. This work was supported by the U.S. Geological Survey and by the U.S. Bureau of Land Management under Memoranda of Understanding AA550-MU7-31, AA551-MU6-29, AA551-MU8-24, AA551-MU8-21, AA551-MU9-4, AA855-MU0-18 and under Interagency Agreement AA551-IA1-17. We thank the referees for their careful reviews of this paper and for one referee's suggestions for computing the wind–current orientation angles in Table 3.

APPENDIX A

Data Analyses

Standard statistical procedures were used to compute the spectral parameters discussed in this paper. The autospectra, coherence and phase computations are described by Fofonoff (1969). To reduce leakage, a Hanning window, with a 50 percent overlap, was applied to each dataset. When there were gaps in the time series, a Fourier transform with a set piece length and a 50 percent Hanning window was computed for each continuous data segment. The combination of Fourier coefficients appropriate to each spectral parameter was then piece-averaged over the segments.

For a given input signal $x(t)$, and output signal $y(t)$, the squared coherence represents the percentage of energy in the output signal that is linearly related to the input signal at frequency f. The amplitude of the transfer coefficient

$$tr(f) = \left(\frac{\gamma^2(f)Ay(f)}{Ax(f)}\right)^{1/2}$$

where γ is the coherence, Ay the output autospectrum, and Ax the input autospectrum at frequency f, is a gain factor. It represents the amplitude of the output signal for a unit input signal. The phase of the transfer coefficient is the same as the phase for coherence. For stable, causal systems the transfer function is also the frequency response function (Bendat and Piersol, 1971). The frequency response function is the transfer function with a purely imaginary exponent (i.e., the exponent of the transfer function, $a + ib$, becomes $i2\pi f$, where f is the frequency). For the data presented in this paper, the two names are equivalent.

The computation of the ellipse orientation and stability is described by Gonella (1972). Each contribution to the orientation is weighted by the foci distance, so circular motions do not affect the result. The ellipse stability indicates how the orientation varies with frequency over the record. High values [O(1)] occur when the orientation is constant. Low values [O(0)] occur when the orientation varies randomly.

To examine the variation of the statistical parameters over the several years of data, the statistical parameters were calculated for sequential two-month data blocks. Occasionally an overlap of 10 days maximum length occurred between the last two sequential segments of a data record. For each two-month segment, the data were Hanned and piece-averaged with a basic piece-length of 528 h. The estimates of the parameters were examined for several frequency bands (at 176 h, 105–264 h, and 58–528 h). Since the parameters had very similar seasonal structures in all three frequency bands, only parameters averaged from 58–528 h are presented in this paper.

The error bars for the spectral quantities were taken from several sources. The autospectra and transfer coefficient error bars are described in Bendat and Piersol (1971). Koopmans (1974) gives the error bars around the phase. The zero significance level for coherence is

$$\gamma_0 = [1 - (0.05)^{1/(p-1)}]^{1/2}$$

where p is the number of independent pieces available in the time series (Julian, 1975).

APPENDIX B

Models for the Predicted Coherence and Veering Angles

If one assumes that the current is driven partly by wind stress and partly by processes incoherent with wind stress, then a simple model can represent the wind–current system. At a particular frequency, let the wind stress and current be represented by

$$W = W$$

$$C = aW + N.$$

Here W is the wind stress and C the current; N is the component of current that is independent of wind stress and a is the transfer coefficient that couples the wind to the current. All quantities are complex. The variance and coherence of the wind and current are

$$WW^* = W^2 \quad \text{(wind-stress variance)}$$

$$CC^* = a^2W^2 + N^2 \quad \text{(current variance)}$$

$$\text{coh}^2 = a^2W^2/(a^2W^2 + N^2) \quad \text{(coherence squared)}.$$

The amplitude of the transfer coefficient can be calculated when the measured coherence is significant (Appendix A). But when the measured coherence is not significant, one can still place upper limits on the transfer coefficient's amplitude. One can either assume that the maximum coherence amplitude present in the system is the 95% zero significance level, then use the measured wind-stress and current variances to compute an upper limit for the transfer coefficient or one can assume a transfer coefficient amplitude A, then calculate the "predicted coherence" [Eq. (1)]. If the predicted coherence is larger than the zero-significance level, then the assumed amplitude A of the transfer coefficient is too large. If the predicted coherence is below the zero-significance level, one cannot reject the initial hypothesis that the transfer coefficient amplitude is A.

In this paper we have used this model to investigate the seasonality of the wind–current coupling. In particular, a major question was: when the wind–current coupling is below the zero-significance level, is this because

1) other processes not related to wind forcing add enough energy to the currents to make the percentage of current energy driven by wind stress statistically insignificant, even though the transfer coefficient's amplitude is constant; or

2) the coupling between wind stress and current decreases.

For example, wind stress was strong in the fall of 1977. If the transfer coefficient amplitude for mid-depth currents was about the same as was observed in winter [around 2.6 $cm^3/(dyn\ s)$], then the wind-driven current variance should have been around 74 $cm^2\ s^{-2}$, given that the wind-stress variance was 3.3 $dyn^2\ cm^{-4}$. Since the measured current was 122 $cm^2\ s^{-2}$, the predicted coherence is 0.78, well above the significance level. The observed coherence was not significant (measured amplitude 0.14). Hence, the amplitude of the transfer coefficient must have been smaller than was observed in winter. In summer, one could not determine whether the transfer coefficient amplitude was smaller than in winter, for the predicted coherence, based on winter amplitudes, was below the zero significance level.

One can also use the wind–current model to estimate a veering angle between wind stress and wind-driven currents. Let the wind stress and wind-driven current vectors be

$$W = W\mathbf{r}$$

$$C = aW\mathbf{m}$$

where $\mathbf{r}$ and $\mathbf{m}$ are unit vectors. In the x, y coordinate system:

$$\mathbf{r} = \cos(\alpha)\mathbf{i} + \sin(\alpha)\mathbf{j}$$

$$\mathbf{m} = \cos(\gamma)\mathbf{i} + \sin(\gamma)\mathbf{j}$$

The angles α and γ are measured counterclockwise from the x axis. The veering angle between wind stress and current ϕ is $(\gamma - \alpha)$. In x, y coordinates:

$$\left.\begin{aligned} W_i &= W\cos(\alpha) \\ W_j &= W\sin(\alpha) \\ C_i &= aW\cos(\gamma) + N \\ C_j &= aW\sin(\gamma) + O \end{aligned}\right\};$$

N and O are the components of currents on the x, y axes that are independent of the wind stress. The four cross-spectral relations between current and wind stress are

$$\left.\begin{aligned} W_i^*C_i &= \text{Co}_{ii} - i\,\text{Qu}_{ii} = \cos(\gamma)\cos(\alpha)[W^*Wae^{i\theta}] \\ W_i^*C_j &= \text{Co}_{ij} - i\,\text{Qu}_{ij} = \sin(\gamma)\cos(\alpha)[W^*Wae^{i\theta}] \\ W_j^*C_i &= \text{Co}_{ji} - i\,\text{Qu}_{ji} = \cos(\gamma)\sin(\alpha)[W^*Wae^{i\theta}] \\ W_j^*C_j &= \text{Co}_{jj} - i\,\text{Qu}_{jj} = \sin(\gamma)\sin(\alpha)[W^*Wae^{i\theta}] \end{aligned}\right\};$$

Co is the cospectrum, Qu the quadrature spectrum, and θ the phase lag between wind and currents. The veering angle ϕ can be estimated from several spectral quantities.

$$\left.\begin{aligned}\tan(\phi) &= (\mathrm{Co}_{ij} - \mathrm{Co}_{ji})/(\mathrm{Co}_{ii} + \mathrm{Co}_{jj})\\ \tan(\phi) &= (\mathrm{Qu}_{ij} - \mathrm{Qu}_{ji})/\mathrm{Qu}_{ii} + \mathrm{Qu}_{jj})\end{aligned}\right\}.$$

If, as is the case in this paper, the vector **r** lies along the x axis,

$$\tan(\phi) = \tan(\gamma) = a_j/a_i$$

where a_i and a_j are the amplitudes of the longshelf and cross-shelf transfer coefficients.

These three formulas were used to estimate the veering angles in Table 3. The formulas do not give the same veering angles at a given site, for some of the cross-spectral amplitudes were estimated from a pair of signals which were not coherent with one another (for example, the longshelf wind stress, longshelf near-surface current pair). Hence, the estimated amplitude is noisy.

In Table 3, the veering angle is the average of the three calculated angles. The range is the minimum and maximum angles.

REFERENCES

Beardsley, R. C., and B. Butman, 1974: Circulation on the New England continental shelf: Response to strong winter storms. *Geophys. Res. Lett.*, **1,** 181–184.

Bendat, J. S., and H. G. Piersol, 1971: *Random Data: Analysis and Measurements Procedures.* Wiley-Interscience, 407 pp.

Brink, K. H., 1982: The effect of bottom friction on low-frequency coastal trapped waves. *J. Phys. Oceanogr.*, **12,** 127–133.

——, 1983: Low-frequency free wave and wind-driven motions over a submarine bank. *J. Phys. Oceanogr.*, **13,** 103–116.

Butman, B., and R. C. Beardsley, 1985: Long-term observations on the southern flank of Georges Bank: Seasonal cycle of currents, stratification, and wind stress. *J. Phys. Oceanogr.*, (submitted).

——, M. A. Noble, J. A. Moody and M. H. Bothner, 1983: Lydonia Canyon dynamics experiment: Preliminary results. Environmental geologic studies on the United States Mid- and North Atlantic Outer Continental Shelf area, 1980–1982, Vol. 3. North Atlantic Region, Final Report to Minerals Management Service, B. A. McGregor, Ed., U.S. Geol. Survey, 8-1–8-93.

Csanady, G. T., 1974: Barotropic currents over the Continental Shelf. *J. Phys. Oceanogr.*, **4,** 357–371.

——, 1982: *Circulation in the Coastal Ocean.* Reidel, 279 pp.

Flagg, C. N., B. A. Magnell, D. Frye, J. J. Cura, S. E. McDowell and R. E. Scarlet, 1982: Interpretation of the physical oceanography of Georges Bank. BLM Final Rep., EG&G Rep. No. 82-B4569, 187 pp.

Fofonoff, N. P., 1969: Spectral characteristics of internal waves in the ocean. *Deep-Sea Res.*, **16,** 58–71.

Gonella, J., 1972: A rotary-component method for analyzing meteorological and oceanographic vector time series. *Deep-Sea Res.*, **19,** 833–846.

Han, G. C., and D. A. Mayer, 1981: Current structure on the Long Island inner shelf. *J. Geophys. Res.*, **86,** 4205–4214.

Isaji, T., M. L. Spaulding and J. C. Swanson, 1981: A three-dimensional hydrodynamic model of wind and tidally-induced flows on Georges Bank. Interpretation of the physical oceanography of Georges Bank. U.S. Dept. of Interior, Bureau of Land Management, Prelim. Rep., Contract AA851-CT1-39,[1] A1–A67.

Julian, P. R., 1975: Comments on "the determination of significance levels of the coherence statistic." *J. Atmos. Sci.*, **32,** 836–837.

Koopmans, L. H., 1974: *The Spectral Analysis of Time Series.* Academic Press, 366 pp.

Moody, J. A., and B. Butman, 1980: Semidiurnal bottom pressure and tidal currents on Georges Bank and in the Mid-Atlantic Bight. U.S. Geol. Surv. Open-File Rep. 80-1137, 24 pp.

——, and Collaborators, 1984: Atlas of tidal elevation and current observations on the northeast American Continental Shelf and Slope. *U.S. Geol. Surv. Bull.* 1611, 122 pp.

Noble, M. A., and B. Butman, 1979: Low-frequency wind-induced sea-level oscillations along the east coast of North America. *J. Geophys. Res.*, **84,** 3227–3236.

——, B. Butman and E. Williams, 1983: On the longshelf structure and dynamics of subtidal currents on the eastern United States Continental Shelf. *J. Phys. Oceanogr.*, **13,** 2125–2147.

Ou, H. W., R. C. Beardsley, D. Mayer, W. C. Boicourt and B. Butman, 1981: An analysis of subtidal current fluctuations in the Middle Atlantic Bight. *J. Phys. Oceanogr.*, **11,** 1383–1392.

Roll, H. U., 1965: *Physics of the Marine Atmosphere.* Academic Press, 426 pp.

Wang, D. P., 1979: Low-frequency sea-level variability in the Middle Atlantic Bight. *J. Mar. Res.*, **37,** 683–696.

Wu, J., 1980: Wind-stress coefficients over sea surface near neutral conditions. *J. Phys. Oceanogr.*, **10,** 727–740.